ELSEVIER

Microporous and Mesoporous Materials 32 (1999) 63–74

MICROPOROUS AND MESOPOROUS MATERIALS

www.elsevier.nl/locate/micmat

Siting of the Cu^+ ions in dehydrated ion exchanged synthetic and natural chabasites: a Cu^+ photoluminescence study

J. Dědeček*, B. Wichterlová, P. Kubát

J. Heyrovský Institute of Physical Chemistry, Academy of Sciences of the Czech Republic, Dolejškova 3, CZ-182 23 Prague 8, Czech Republic

Received 18 May 1998; received in revised form 19 April 1999; accepted for publication 26 April 1999

Abstract

Cu^+ emission spectra of Cu^{2+} ion exchanged and reduced natural and synthetic CuNa-, CuCa-, CuCs- and CuBa-chabasites were used to identify cationic sites of the Cu^+ luminescence centres in this zeolite. Two different Cu^+ emission bands with maxima at 500 and 540 nm were observed; the emission at 540 nm prevailed at higher Cu loadings. The concentration dependence of the intensity of 500 and 540 nm emission bands indicated that both bands correspond to the single Cu^+ ions. The effect of the presence of co-cations in Cu-chabasites on the luminescence spectra was employed for the identification of the cationic sites corresponding to the individual emission bands. Cu^+ emission at 500 nm reflects the Cu^+ ion located at the cationic site in the eight-membered ring. Cu^+ emission at 540 nm is attributed to the Cu^+ ion coordinated to three oxygen atoms of the regular six-membered ring. The Cu^+ ion in this site is suggested to be located above the six-ring plane, similar to the siting of Cu^+ ions in Y zeolite.

Keywords: Cation siting; Cu-chabasite; Cu^+ emission; Luminescence

1. Introduction

Zeolites containing Cu ions attract attention owing to their high catalytic activity in NO [1–5] and N_2O decomposition [6] and selective catalytic reduction (SCR) of NO with ammonia [7–9] and hydrocarbons [10–12]. The Cu^+ ions were suggested [13] to be catalytic centres in NO and N_2O decompositions. The essential question is the structure of the reaction centres. Recently, a cationic site of the Cu^+ ions active in the NO decomposition over Cu–ZSM-5 was proposed [14,15]. But there is still a lack of general information on the siting and coordination of the Cu^+ ions in zeolites.

With aluminium-rich zeolites, such as chabasite, faujasite and A-type zeolites, the cationic sites of the Cu^{2+} ions are known [16–19]. This knowledge is based on the results of X-ray diffraction (XRD) experiments, but this technique does not, in principle, allow the determination of the oxidation state of the cations (since they have similar electron density functions), thus bringing difficulties in the identification of the Cu^+ ion siting. For zeolites with a low aluminium content, such as ZSM-5, ferrierite and beta, which are not suitable for XRD investigations, there is a complete lack of information on the cation siting in these structures.

* Corresponding author.
E-mail address: dedecek@jh-inst.cas.cz (J. Dědeček)

1387-1811/99/$ – see front matter
PII: S1387-1811(99)00090-6

Emission spectroscopy has been found to be a powerful tool for characterisation of the Cu^+ ions incorporated in zeolites [20–23], but the assignment of the observed Cu^+ emission bands to *defined* Cu^+ *species is not yet resolved*. The main interest was focused on the Cu ions exhibiting an emission band at 540 nm, which was suggested to be a catalytic centre in NO decomposition in high-silica zeolites [14,23]. Recently, we reported that this 540 nm emission band can represent two different centres with different types of luminescence kinetics: one of them exists in high-silica zeolites, and the other is connected with aluminium-rich zeolites [14,23]. Strome and Klier [21,24] attributed the Cu^+ emission at 540 nm in faujasite to the single Cu^+ ion located in the regular six-ring of site I′. Cu^+ ions located in this site exhibit C_{3v} symmetry of the ligand field of framework oxygen atoms. This suggestion was based on the XRD data of the Cu^{2+} siting in Y zeolite [17]. On the other hand, Anpo and coworkers [25,26] attributed the Cu^+ ion emission at 510 nm to the single Cu^+ ion and the emission band at 540 nm was ascribed to bridging $Cu^+\cdots Cu^+$ species. Their suggestion was based on the EXAFS study of Cu^+-Y zeolites.

Also, factors controlling the emission wavelength of the Cu^+ ions located in zeolite matrices are not well established. The model proposed by Texter et al. [27] explains the different wavelengths emitted by the Cu^+ ion implanted in various matrices by the repulsion of the Cu^+ excited state by the surrounding lattice. But, with regard to the zeolite structural and compositional features, this model does not allow identification of the mechanism controlling the repulsion of the Cu^+ ions in zeolites. Both the changes of the symmetry and strength of the ligand field (LF) of the single Cu^+ ion or induced changes of the LF by the formation of the $Cu^+\cdots Cu^+$ species affect the repulsion of the Cu^+ excited state, i.e. the Cu^+ emission wavelength.

In the present paper, the structure of chabasite is used to elucidate the origin of the emission bands at 500 and 540 nm. Both the Cu^+ emission bands are attributed to the single Cu^+ ions, the band at 500 nm to the Cu^+ located in the eight-membered ring, and the band at 540 nm to the Cu^+ ion located in the regular six-membered ring. This assignment was based on a comparison of the observed dependence of the intensity of the individual emission bands on the Cu concentration and on the effect of the presence of non-transition metal co-cations with known siting on the Cu^+ emission spectra.

2. Experimental

2.1. Zeolite preparation

The synthesis of chabasite was performed according to the procedure of Gaffney [28]. *Zeolite* Y (Si/Al = 2.7) in ammonium form was used as a source material and was mixed with a solution of potassium hydroxide. The batch composition was $0.17Na_2O{:}2.0K_2O{:}Al_2O_3{:}5.4SiO_2{:}224H_2O$. The synthesis took place in a polypropylene bottle with a screw-top lid at a temperature of 368 K for 96 h *without agitation. After synthesis, the product* was recovered by filtration, washed repeatedly with deionised water and dried at ambient temperature. The crystallinity and phase purity were determined using a Siemens D5005 X-ray powder diffractometer with CuKα radiation and Ni filter in the range of 2θ of 5–50°. The diffraction pattern is *depicted in Fig. 1*(a).

Synthetic chabasite and natural sedimentary chabasite from North Korea — chemical composition (weight percent) 63.89% SiO_2, 17.48% Al_2O_3, 8.37% Fe_2O_3, 5.15% K_2O, 3.10% CaO, 1.21% MgO, 0.40% TiO_2 and 0.39% Na_2O [the XRD pattern is given in Fig. 1(b)] — were equilibrated *four times with 0.5 M NaCl (20 ml of solution per* 1 g of zeolite) for 12 h. After the ion exchange, the Na-chabasites were washed with distilled water and dried at room temperature. Ca-, Ba- and Cs-chabasites were prepared by the equilibration of Na-chabasite with 0.1 M $Ca(NO_3)_2$, $Ba(NO_3)_2$ and CsCl solutions respectively. These zeolites *were washed with distilled water and dried at* ambient temperature. The conditions of Ca^{2+}, Ba^{2+} and Cs^+ ion exchanges are given in Table 1.

Cu^{2+}-chabasite samples with Cu concentrations varying from 0.20 to 7.60 wt% were prepared by

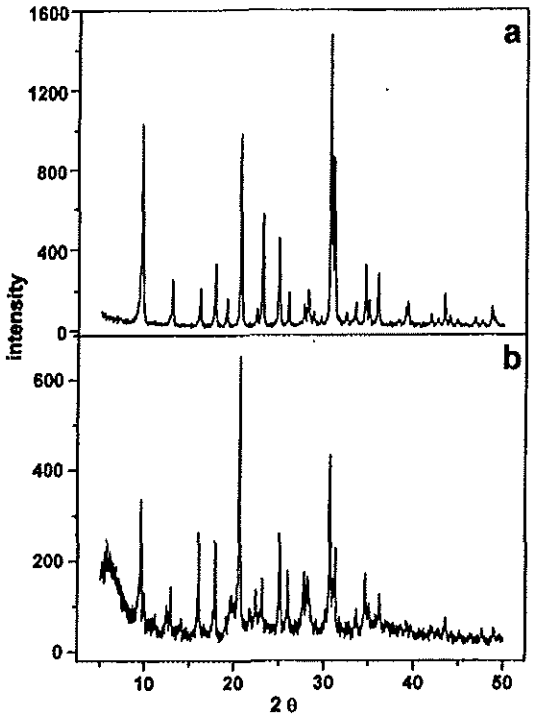

Fig. 1. XRD patterns of (a) synthetic (b) natural sedimentary chabasites.

Table 1
Preparation conditions for Cs^+-, Ca^{2+}- and Ba^{2+}-chabasites

Zeolite[a]	Solution/zeolite (ml/g)	Exchange time (h)
CsNa-CHAB/N	40	6
	60	12
BaNa-CHAB/N	40	6
	60	12
CaNa-CHAB/N	40	6
	80	10
CaNa-CHAB/S	80	3
	80	12

[a] N: natural sedimentary chabasite; S: synthetic chabasite.

the ion exchange of Na-, Ca-, Cs- and Ba-chabasites with aqueous solutions of Cu acetate. The pH of Cu-acetate–chabasite solutions varied during the Ion exchange procedure from 5.1 to 5.6. Samples were carefully washed with distilled water, dried at ambient temperature and grained. Detailed conditions of the sample preparations and chemical compositions of Cu-chabasites are given in Tables 2 and 3.

2.2. Cu^+ emission

Prior to monitoring of the Cu^+ photoluminescence spectra, the Cu^{2+} zeolites were calcined in an oxygen stream at 350°C for 3 h to remove all traces of organic compounds from the zeolite, well known as Cu^+ luminescence quenchers [21,24,28]. Then, they were dehydrated at 450°C with subsequent reduction in hydrogen of 4×10^3 Pa for 20 s up to 64 min at 450°C or in carbon monoxide of 5.3×10^3 Pa for 40 min at 450°C. The intensity of the Cu^+ emission depended not only on the Cu/Al zeolite composition, but also on the time of the reduction, as is described in Section 3. For determination of the distribution of the Cu^+ ions in chabasite, the samples were reduced in hydrogen at conditions yielding maximum concentrations of the monovalent copper. Under the chosen conditions, 90% of the copper in the zeolite was in a monovalent state and no significant amounts were reduced to the zero-valent copper, as was proven by DR UV–VIS spectra (not shown here). After the reduction of Cu^{2+} zeolites, the samples were evacuated at the temperature of reduction for 15 min, transferred under vacuum to the silica cell and sealed. The details of the reduction procedure of divalent to monovalent copper, which have been described in detail elsewhere [23,29–31], are discussed below.

Cu^+ emission spectra were recorded using a nanosecond laser kinetic spectrometer (Applied Photophysics). Cu^+-zeolites were excited by the laser beam of the XeCl excimer laser (Lambda Physik 205, emission wavelength 308 nm, pulse width 28 ns, pulse energy 100 mJ). The 320 nm filter was situated between a 2 mm thick silica cell and the monochromator. The emission signal was detected with an R 928 photomultiplier (Hamamatsu), recorded with a PM 3325 oscilloscope and processed by computer. All the luminescence measurements were carried out at room temperature. The Cu^+ emission spectra were constructed from the values of luminescence intensity at the individual wavelengths of emission at selected times after excitation (2, 5, 10, 20, 50, 100

Table 2
Preparation conditions for Cu^{2+}-chabasites

Zeolite[a]	Cu/Al	Cu concentration in solution (M)	Solution/zeolite (ml/g)	Exchange time (h)
CuNa-CHAB/N	0.01	0.001	25	3
CuNa-CHAB/N	0.11	0.005	25	3
CuNa-CHAB/N	0.17	0.01	50	9
CuNa-CHAB/N	0.28	0.01	100	17
CuNa-CHAB/N[b]	0.34	0.01	80+80	3+12
CuNa-CHAB/N[b]	0.38	0.1	12+20	3+14
CuNa-CHAB/S	0.01	0.001	25	1
CuNa-CHAB/S	0.08	0.005	65	1
CuNa-CHAB/S	0.15	0.01	60	3
CuNa-CHAB/S	0.22	0.01	110	12
CuNa-CHAB/S[b]	0.32	0.01	110+110	3+15
CuCs-CHAB/N	0.05	0.01	40	1
CuCa-CHAB/N	0.10	0.01	40	1
CuBa-CHAB/N	0.09	0.01	40	1
CuCa-CHAB/S	0.03	0.01	45	1.5

[a] N: natural sedimentary chabasite; S: synthetic chabasite.
[b] Two-step ion exchange.

Table 3
Chemical compositions of Cu^{2+}-chabasites

Zeolite[a]	Cu/Al	Me/Al[b]	Ca/Al	Na/Al	K/Al	Mg/Al	Fe/Al	Ti/Al
Na-CHAB/N	–	–	0.11	0.43	0.15	0.06	0.30	0.02
Na-CHAB/S	–	–	0.01	0.94	–	–	0	–
CuNa-CHAB/N	0.01	–	0.11	0.40	0.15	0.06	0.30	0.02
CuNa-CHAB/N	0.11	–	0.08	0.25	0.13	0.03	0.30	0.01
CuNa-CHAB/N	0.17	–	0.09	0.22	0.13	0	0.33	0.01
CuNa-CHAB/N	0.28	–	0.07	0.17	0.13	0	0.33	0.03
CuNa-CHAB/N	0.34	–	0.05	0.12	0.14	0	0.35	0.02
CuNa-CHAB/N	0.38	–	0.07	0.08	0.14	0	0.31	0.02
CuNa-CHAB/S	0.01	–	–	0.99	–	–	–	–
CuNa-CHAB/S	0.08	–	–	0.84	–	–	–	–
CuNa-CHAB/S	0.15	–	–	0.68	–	–	–	–
CuNa-CHAB/S	0.22	–	–	0.51	–	–	–	–
CuNa-CHAB/S	0.32	–	–	0.26	–	–	–	–
CuCs-CHAB/N	0.05	0.42	0	0.03	0.11	0.08	0.29	0.02
CuBa-CHAB/N	0.09	0.25	0.04	0.03	0.11	0.02	0.33	0.02
CuCa-CHAB/N	0.10	–	0.19	0.08	0.11	0	0.30	0.02
CuCa-CHAB/S	0.03	–	0.41	0.06	–	–	–	–

[a] N: natural sedimentary chabasite; S: synthetic chabasite.
[b] Me/Al is Cs/Al for CuCs-chabasite and Ba/Al for CuBa-chabasite.

and 200 μs) using the Applied Photophysics Kinetic Spectrometer software. Decomposition of the luminescence spectra to the Gaussian curves and final data processing was carried out using the Microcal Origin 4.1 software (Microcal Software).

3. Results

Typical emission spectra of the Cu^{+}Na-chabasite are shown in Fig. 2. Both the asymmetry of the emission spectrum and its shift

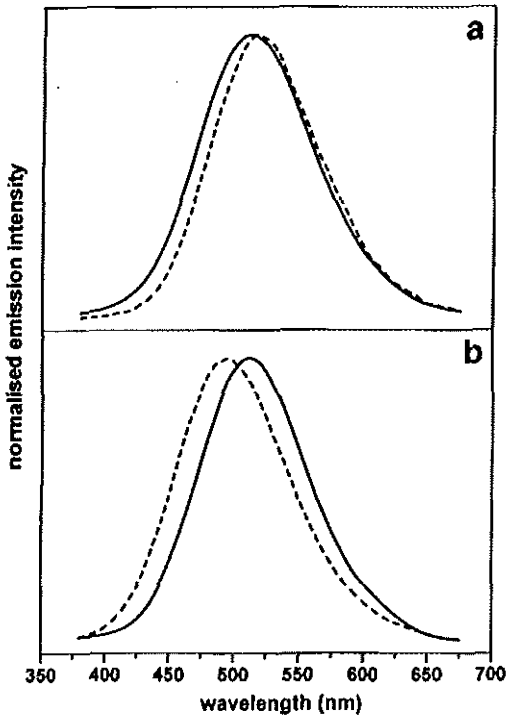

Fig. 2. (a) Normalised intensity of the Cu^+ emission of Cu^+-chabasite (Cu/Al = 0.38) recorded at 2 (—) and 100 μs (– –) after excitation. Cu^{2+}-chabasite was reduced in hydrogen of 4×10^3 Pa for 2 min at 450°C. (b) Effect of reduction time of the Cu^+-chabasite (Cu/Al = 0.38) on the normalised Cu^+ emission intensity. Cu^{2+}-chabasite was reduced in hydrogen of 4×10^3 Pa for 1 (—) and 64 min (– –) at 450°C.

to a longer wavelength with increasing time after excitation indicated the presence of at least two emission bands with different luminescence decays [Fig. 2(a)]. This was also indicated by the maximum shifts to shorter wavelengths with increasing reduction time [Fig. 2(b)]. These shifts reflected the presence of different Cu^+ luminescence centres exhibiting different reducibilities in the $Cu^{2+} \rightarrow Cu^+ \rightarrow Cu^0$ process. Decomposition of the emission spectra of CuNa-chabasites to the Gaussian bands and second derivative mode analysis (not shown in Fig. 2) showed the presence of two emission bands with maxima at 500 ± 5 and 540 ± 5 nm, as illustrated in Fig. 3. The decomposition of the Cu^+ luminescence spectra to the Gaussian bands was discussed in detail elsewhere [22,23].

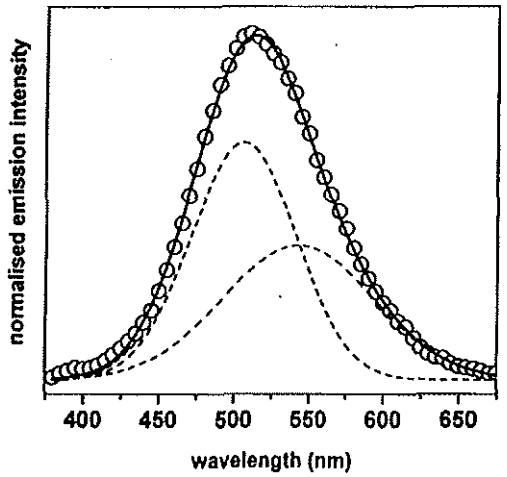

Fig. 3. Decomposition of the emission spectrum of Cu^+-chabasite (Cu/Al = 0.38) to Gaussian bands: Cu^+ emission spectrum (O); resulting fit to the Gaussian curves (—); Gaussian curves composing spectrum (– –). Cu^{2+}-chabasite was reduced in hydrogen of 4×10^3 Pa for 2 min at 450°C.

The decay of the Cu^+ emission intensity at 500 nm is documented in Fig. 4, where the normalised luminescence decay is shown. The dependence of the luminescence intensity on time followed a double-exponential dependence, described by

$$I = I_0[a_1 \exp(-t/\tau_1) + a_2 \exp(-t/\tau_2)], \quad (1)$$

where I is the luminescence intensity at time t ($t = 0$ for time of excitation), I_0 is the initial luminescence intensity, τ_1 and τ_2 are luminescence decay times and a_1 and a_2 are pre-exponential factors. The emission centre with an emission at 500 nm, both for the natural and synthetic chabasite, was characterised by the decay times 10 ± 5 and 80 ± 10 μs; the lower one represents the life time of the lowest excited state and is used as a characteristic of the Cu^+ ion located in a zeolite (see Refs. [22,23,30]). Owing to the strong overlap of the emission band at 540 nm by the band at 500 nm, its decay time could not be estimated. However, the 540 nm luminescence prevails in the spectra recorded at a longer time after the excitation compared with that recorded at 2 μs; the decay time of the 540 nm emission is substantially longer than that of the 500 nm emission.

In order to determine the distribution of the two Cu^+ species in chabasite, it was necessary to

DOCKET ALARM

Explore Litigation Insights

Docket Alarm provides insights to develop a more informed litigation strategy and the peace of mind of knowing you're on top of things.

Real-Time Litigation Alerts

Keep your litigation team up-to-date with **real-time alerts** and advanced team management tools built for the enterprise, all while greatly reducing PACER spend.

Our comprehensive service means we can handle Federal, State, and Administrative courts across the country.

Advanced Docket Research

With over 230 million records, Docket Alarm's cloud-native docket research platform finds what other services can't. Coverage includes Federal, State, plus PTAB, TTAB, ITC and NLRB decisions, all in one place.

Identify arguments that have been successful in the past with full text, pinpoint searching. Link to case law cited within any court document via Fastcase.

Analytics At Your Fingertips

Learn what happened the last time a particular judge, opposing counsel or company faced cases similar to yours.

Advanced out-of-the-box PTAB and TTAB analytics are always at your fingertips.

API

Docket Alarm offers a powerful API (application programming interface) to developers that want to integrate case filings into their apps.

LAW FIRMS
Build custom dashboards for your attorneys and clients with live data direct from the court.

Automate many repetitive legal tasks like conflict checks, document management, and marketing.

FINANCIAL INSTITUTIONS
Litigation and bankruptcy checks for companies and debtors.

E-DISCOVERY AND LEGAL VENDORS
Sync your system to PACER to automate legal marketing.